Physics – Uspekhi **56** (3) 261 – 268 (2013) ©2013 Uspekhi Fizicheskikh Nauk, Russian Academy of Sciences

REVIEWS OF TOPICAL PROBLEMS PACS numbers: 61.43.Dq, **62.25.–g**, 81.05.Kf, **81.07.–b**

Metallic nano/microglasses: new approaches in nanostructured materials science

R A Andrievski

DOI: 10.3367/UFNe.0183.201303c.0277

Contents

Abstract. This paper reviews the state of the art in metallic nano/microglasses, with a focus on their preparation methods, structure, and physical/mechanical properties. Characterization methods for these glasses are reviewed together with how size effects, temperature variation, and ion irradiation contribute to the increase in their ductility. Some aspects that require more detailed study are identified.

1. Introduction

The attention of physicists, chemists, and material scientists has been focused on amorphous materials for over 70 years (see, e.g., [1–20]). Studies of these objects, characterized by a random structure devoid of long-range order and showing a wide spectrum of transport, magnetic, and mechanical properties, have greatly contributed to our understanding of the nature of the condensed state of matter. On the other hand, the high level of their physicomechanical properties, including high corrosion resistance, have been impetus for extensive material science and technological research on the methods of fabrication and application of these materials.

Novel approaches to the preparation of amorphous and amorphous–nanocrystalline materials applicable to nanoglasses and suitable for increasing the ductility of metallic glasses have recently been proposed. This review is designed to analyze these trends (also briefly discussed in Ref. [21]).

R A Andrievski Institute of Problems of Chemical Physics, Russian Academy of Sciences,
Prosp. Akad. Semenova 1, 142432 Chernogolovka, Moscow region, Russian Federation
Tel. +7 (496) 522 77 93
Fax +7 (496) 522 35 07
E-mail: ara@icp.ac.ru

Received 11 April 2012, revised 1 June 2012
Uspekhi Fizicheskikh Nauk **183** (3) 277 – 285 (2013)
DOI: 10.3367/UFNr.0183.201303c.0277
Translated by Yu V Morozov; edited by A M Semikhatov

2. Nanoglasses

2.1. Methods of preparation

Metallic glasses are amorphous materials based on metals such as Cu, Ni, Fe, Au, Pd, Ti, Zr, Be, and La, not infrequently doped with non-metals (B, Si, P, etc). Hardening a metal strip from the melt on a moving substrate at a rate $\geqslant 10^6$ K s^{-1}, thermal film deposition onto cooled substrates, and electrodeposition are traditional methods for the fabrication of metallic glasses, giving rise to disordered structures due to the formation of multiple nucleation sites and a slowdown in their growth. Preparation of so-called bulk metallic glasses (BMGs) up to a few centimeters in size by thermoplastic forming is described in great detail in Ref. [17].

Totally different methods for obtaining nanomaterials of a new type, i.e., nanoglasses with a tunable atomic structure, have been proposed. As is known, the main idea of nanomaterials put forward in the work of Gleiter and coworkers [22–24] was to considerably increase the fraction of regions with a disordered structure in a crystalline material (grain boundaries, triple junctions, and interfaces) as a major tool for substantially modifying the properties of solids by altering their overall and electronic structures. Further consideration of the importance of interfaces for preparing metallic nanoglasses brought about the scheme presented in Fig. 1 [25–27], illustrating thermal delocalization of interfaces among four amorphous nanoparticles A, B, C, and D. Their annealing resulted in interface and free volume expansion (situations 'a' and 'b'), leading to complete delocalization at the final stage (situation 'c'). This scheme differs from the behavior of interfaces in crystalline nanoparticles, leading to a decrease in the free volume and refinement of intergrain boundaries.

Experimental studies with a number of compactified amorphous nanoparticles (Au–Si, Au–La, Fe–Si, La–Si, Pd–Si, Ni–Ti, Ni–Zr, and Ti–P) with the use of X-ray photoelectron spectroscopy (XPS) and Mössbauer spectroscopy [25, 27, 28] confirmed the soundness of the scheme presented in Fig. 1.

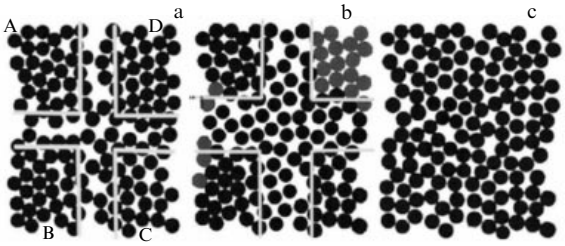

Figure 1. Schematic drawing of interface behavior during annealing of nanoglasses [27]. The notation is explained in the text.

Molecular dynamics methods were used to reveal peculiarities in the behavior of amorphous nanoparticles of Ge and $Cu_{64}Zr_{36}$ during high-pressure consolidation [29, 30]. Interface expansion with the formation of an excess free volume was revealed by simulating compactification of 32 Ge nanoparticles (5 nm) at 5 GPa ($T = 300$ K) [29]. Figure 2 schematically shows variants of the pressure effect on the interface structure of (a) crystalline nanoparticles, (b) metallic nanoglasses, and (c) BMG [30]. Intergrain boundaries in the case of compactification of crystalline nanoparticles are characterized by small free volume (Fig. 2a). Compactification of amorphous nanoparticles and BMG deformation are accompanied by the appearance of an excess free volume, as shown in Figs 2b and c (in the latter case, due to the formation of shear bands).

The generation of shear bands under deformation of metallic glasses was observed in many experiments but was especially exemplified in the case of severe plastic (or megaplastic) deformations (SPDs) of a specially selected BMG, $Au_{49}Ag_{5.5}Pd_{2.3}Cu_{26.9}Si_{16.3}$, which does not undergo nanocrystallization under SPD conditions [31]. Figure 3a, b shows SEM and TEM images of transverse fractures in this glass after SPD (five revolutions of HPT straining at 6 GPA), suggesting the formation of multiple shear bands. The free volume in the atomic packing of amorphous nanoparticles before and after SPD is schematically depicted in Fig. 3c, d [31].

Studies based on a synchrotron source showed that transverse distribution functions for intact and deformed BMG samples are subject to marked variation and the level of short-range order decreases after the SPD, thus giving additional evidence of the free volume enlargement [31]. We note that the use of SPD methods (high-pressure torsion, equal-channel angular pressing, etc.) [32] significantly extends the potential of nanotechnologies and nanoscale materials science. For example, the deformation of amorphous $Ti_{50}Ni_{25}Cu_{25}$ alloy in a Bridgeman chamber (4 GPa) after 9 revolutions resulted in cyclic amorphous–crystalline phase transitions with the formation and dissolution of nanocrystals [33]. There is every reason to believe that SPD techniques will be extensively used to fabricate metallic glass-based materials.

Preparation of nanowires, nanospheres, and nanofilms from BMG has recently been reported [34–38]. Figure 4 shows SEM images of nanostructures arising on strain cleavage surfaces of various BMGs. Such structures are believed to result from deformation in shear band regions, where increased temperature causes the formation of liquid interlayers and intense mass transfer. Investigations into details of mechanisms of nanostructure formation in shear band regions are underway.

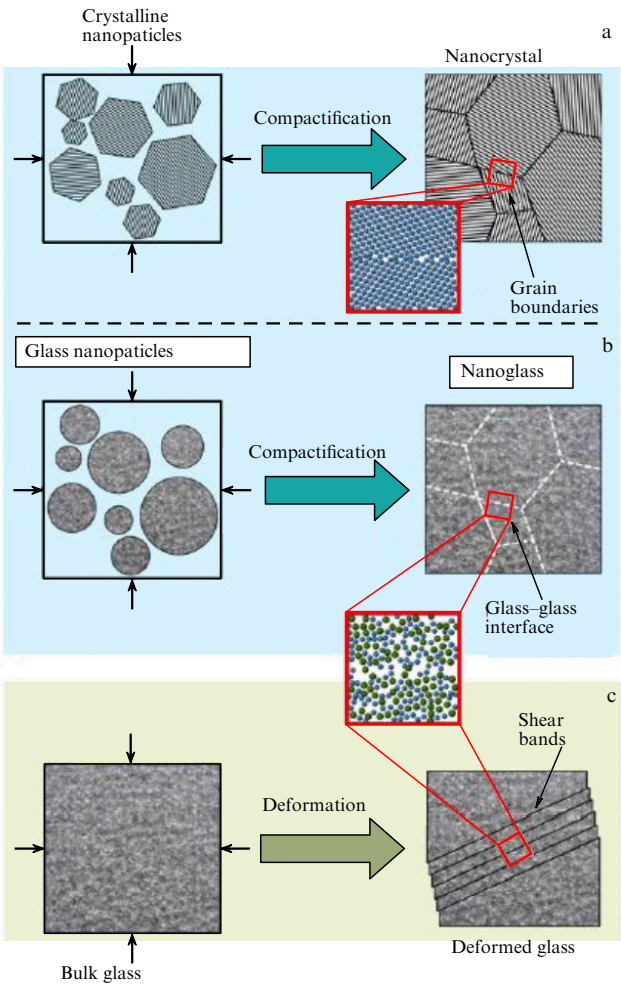

Figure 2. Pressure effect on the structure of interfaces in (a) crystalline nanoparticles, (b) amorphous (glass) nanoparticles, and (c) BMG [30].

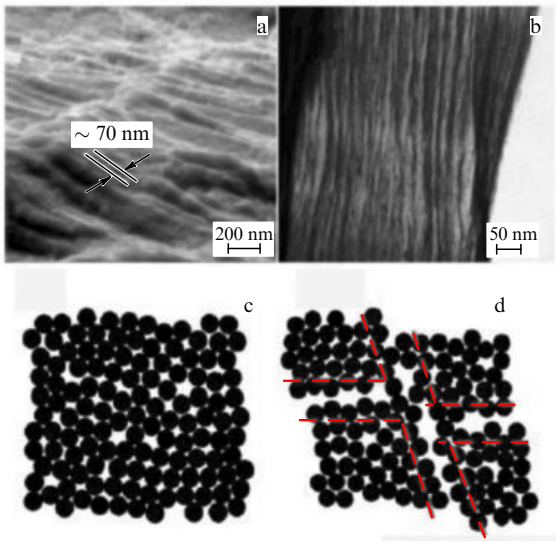

Figure 3. (a) SEM and (b) TEM images of a cross section through the $Au_{49}Ag_{5.5}Pd_{2.3}Cu_{26.9}Si_{16.3}$ BMG after SPD by HPT. Schematic drawing of the two-dimensional nanoparticle packing in metallic glasses showing (c) the free volume before SPD and (d) the generation of high-density shear bands after SPD [31].

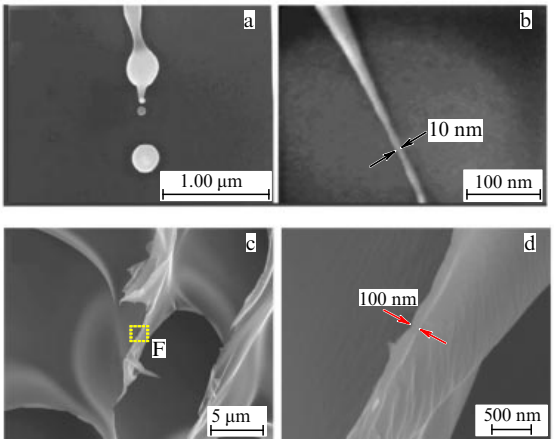

Figure 4. SEM images of $Zr_{50}Cu_{40}Al_{10}$ BMG fractures: (a) spherical nanodroplets near the tip of a nanowire; (b) nanowire [34] and $Zr_{41.2}Ti_{13.8}Cu_{10}Ni_{12.5}Be_{22.5}$; (c) shear strain region, (d) 100 nm thick nanofilm (magnified F section) [38].

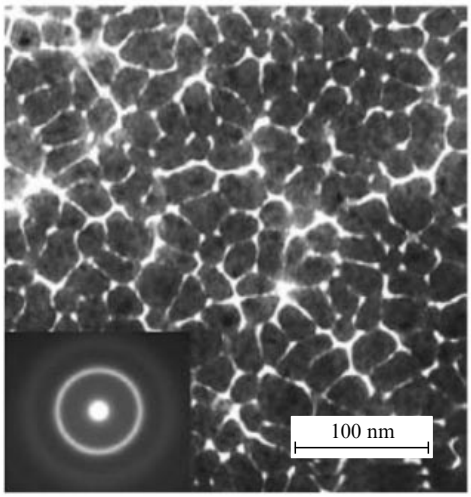

Figure 5. Light-field electron micrograph of an $Au_{49}Ag_{5.5}Pd_{2.3}Cu_{26.9}Si_{16.3}$ metallic nanofilm (the inset shows an electron microgram) [39].

A promising method for fabricating $Au_{52}Ag_5Pd_2Cu_{25}Si_{10}Al_6$ metallic glass films by magnetron sputtering of powder targets under strict control of their amorphous character and structure has been proposed in Ref. [39]. Figure 5 is a light-field TEM image of a metallic glass film and an electron microgram exhibiting an amorphous structure. Such amorphous structures, unlike crystalline ones, are termed nanogranulated and have 0.8–1.2 nm glass–glass interfaces [40]. The size of consolidated granules varies from ~ 10 to 30 nm or more, depending on the gold content in the initial targets and the spraying duration.

2.2 Attestation and properties

As in the study of nanomaterials, a variety of methods are used to characterize specific structural features of nanoglasses: diffraction and scattering of electrons, X-rays, and neutrons (including electron microphotography of selected portions and diffraction at small scattering angles); SEM and TEM (including high-resolution (HR) methods); atomic force microscopy (AFM); RPS; positron annihilation; energy dispersive spectroscopy; Mössbauer spectroscopy; densitometry; desorptiometry; and differential scanning calorimetry. The combined application of these techniques is reported in many articles (see, e.g., [25, 39, 40]). The use of several independent methods is an indispensable prerequisite for obtaining representative information about free volume localization and delocalization and the structural specificity of metallic nanoglasses.

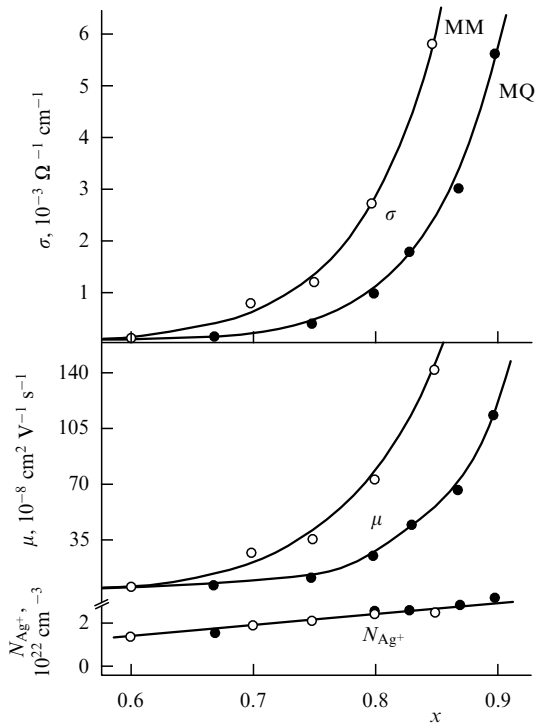

Figure 6. Variations of conductivity (σ), mobility (μ), and concentration of Ag^+ ions (N_{Ag^+}) in the $xAg_2S-(1-x)Sb_2S_3$ system: ○ — samples obtained by high-energy milling (MM), ● — samples obtained by the melt spinning technique (MQ) [42].

Interface delocalization in nanoglasses allows introducing a variety of defects into these objects, which is impossible using conventional crystalline materials. For example, the dislocation density in the case of plastic deformation is roughly 10^{12} cm^{-2}, corresponding to approximately 1% of the dislocation nuclei regarded as defects [25]. At the same time, Cu–Zr nanoglasses have a relative density of ~ 85% of the initial value; this means that the number of defects in this case is much greater than in deformed metals [25, 29]. Importantly, defects in nanoglasses are distributed over the entire volume.

The presence of the excess free volume is most clearly manifested in transfer phenomena. As shown in [25], the diffuse mobility of Fe^{57} in $Fe_{40}Ni_{40}B_{20}$ metallic glasses increased almost 10-fold as the density changed by 0.8%. Observation of silver and iron isotope diffusion in $Pd_{40}Ni_{40}P_{20}$ BMG at 473 K revealed a difference of almost eight orders of magnitude between the diffusion coefficients for deformed and intact samples [41]. Experimental conditions excluded the possibility of crystallization; therefore, the observed significant enhancement of mobility (compared with bulk diffusion) was attributed to the presence of the free volume in deformation shear bands.

Delocalization of defects in ionic nanoobjects and transition from crystalline structures to amorphous ones are also accompanied by an increase in ionic conductivity [25, 42].

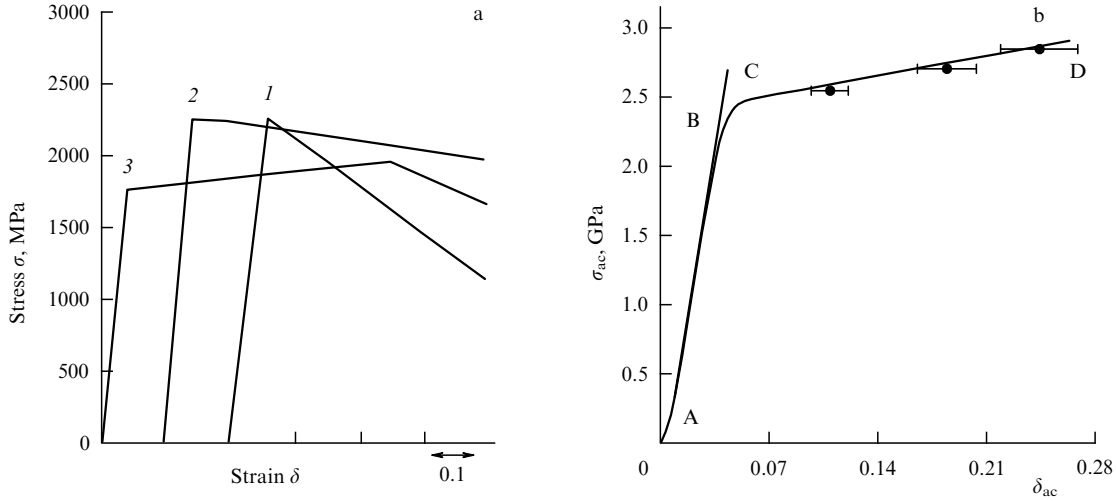

Figure 7. (a) A typical strain diagram of micropillars 330 (*1*), 568 (*2*), and 875 nm (*3*) in diameter and (b) diagram of the actual stress σ_{ac} and actual strain δ_{ac} of a micropillar of Zr-based metallic glass 100 nm in diameter (AB, elastic portion, CD, strain hardening) [47].

Figure 6 shows variations of the conductivity, mobility, and concentration of Ag^+ ions in an amorphous ionic conductor based on the $xAg_2S-(1-x)\,Sb_2S_3$ sulfide system [42]. These data indicate that increasing the silver sulfide level increases the conductivity, mobility, and concentration of silver ions in a manner far from being additive, with the difference more pronounced in samples obtained by high-energy ball milling (MM), which have a more fine-grained structure than those obtained by the ordinary melt spinning technique (MQ).

More information on the mechanical properties of metallic nanoglasses is beginning to accumulate. Nanoindentation of an $Au_{52}Ag_5Pd_2Cu_{25}Si_{10}Al_6$ film revealed its high degree of hardness (5.3 ± 0.1 GPa) and Young modulus (~ 78.8 GPa) in excess of these values for usual BMGs [39]. The hardness of $Sc_{75}Fe_{25}$ metallic nanoglass proved to be 4.57 ± 0.66 GPa, i.e., also somewhat higher than the 4.23 ± 0.36 GPa for BMG [43]. Microcompression testing demonstrated that $Sc_{75}Fe_{25}$ metallic nanoglasses have ductility with a somewhat enhanced breaking stress (up to 1950 MPa), unlike ordinary hardened ribbon samples of the same composition showing a purely elastic behavior and undergoing brittle fracture [40, 43]. Such a difference and specific post-annealing behavior correlate with the results of calculations by the molecular dynamics method and correspond to the concept of critical influence of the number of shear bands as free-volume accumulators.

One more important feature discovered in $Sc_{75}Fe_{25}$ metallic nanoglasses — their ferromagnetic behavior in which they differ from usual hardened ribbon samples showing paramagnetic behavior — is mentioned in [39]. S-shaped magnetization curves of metallic nanoglasses about 8 nm in size are typical of ferromagnets [44].

The high catalytic activity of metallic nanoglasses can be attributed to the presence of many interfaces, as shown in experimental studies demonstrating substantial intensification of the interaction between organosilicon compounds (like dimethylphenyl silanol) and water vapor [39].

By no means can all the above experimental findings be unambiguously explained in terms of the current theory of structure and composition of nanomaterials and nanoglasses. Further studies are needed to clarify the results obtained thus far.

3. Deformation of metallic glasses

3.1 Size effects

Brittle fracture, characteristic of metallic glasses and of many other nanomaterials, significantly narrows the spectrum of their application. We scrutinized the role of size effects as factors influencing the strength and ductility of nanomaterials in a previous paper [45]; here, this issue is considered with reference to BMG and nanoglasses.

Imparting elastic properties to metallic glasses as materials of high mechanical strength and corrosion resistance is a long-discussed issue [14, 46]. These materials are believed to undergo inhomogeneous deformation with the formation of localized shear bands and their rapid propagation, leading to the sample (product) destruction. Most metallic glasses behave like typical brittle materials, although they sometimes show ductility even when stretched. Homogeneous deformation manifests itself at low stress as preceding the shear band formation and also at high temperatures, e.g., at the glass-transition temperature T_g or higher.

Thorough in situ investigations of homogeneous and inhomogeneous deformations in tensile, compressive, and bending tests of metallic glasses in the form of micropillars 10^2-10^3 nm in height and a few micrometers in diameter were conducted with the use of TEM and SEM [47, 48]. These samples were prepared from bigger ones by focused electron-beam-induced etching. Figure 7 shows a diagram of micropillar deformation in a tensile test experiment at room temperature. Figure 8 demonstrates the influence of diameter on the flow stress of zirconium-based metallic glasses ($Zr_{35}Ti_{30}Co_6Be_{29}$ [47], $Zr_{50}Ti_{16.5}Cu_{15}Ni_{18.5}$ [48], and $Cu_{47}Ti_{33}Zr_{11}Ni_6Sn_2Si_1$ [48]).

Figures 7a, b and 8a show that a decrease in diameter leads to a higher flow stress in tensile tests and to a marked change of the strain diagram. Moreover, a sample 100 nm in diameter behaves like a typical metal (Fig. 7b) in that it undergoes some strain strengthening and has a ductility equivalent to 25% of the actual strain (roughly corresponding to 7% of the measured relative elongation upon destruction); the actual breaking stress is ~ 2.8 GPa. Also, it was shown in Ref. [47] that a 100 nm sample underwent

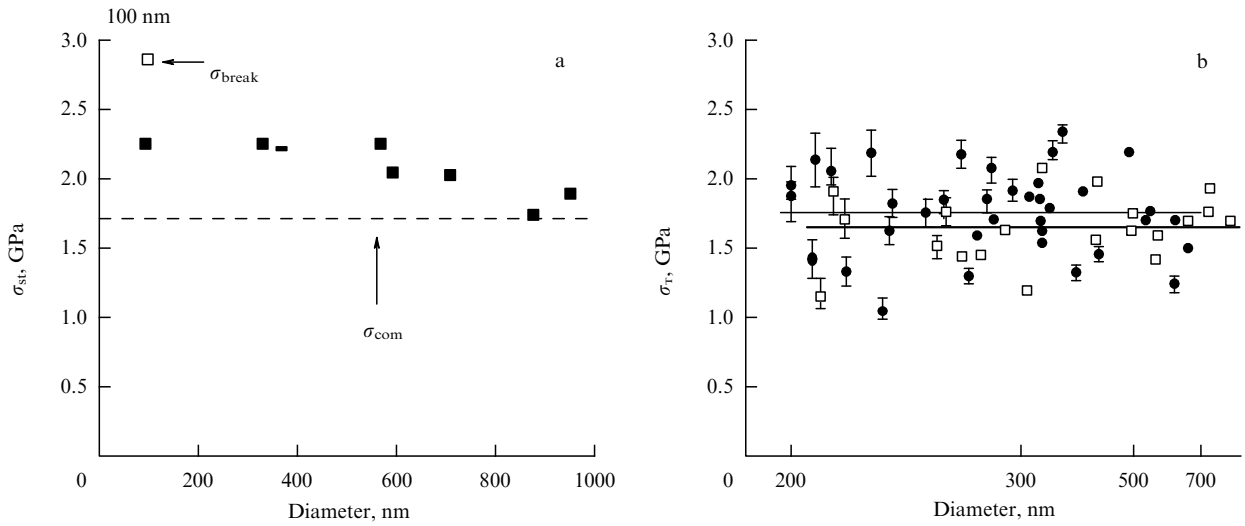

Figure 8. (a) Influence of the micropillar diameter on the flow stress σ_{st} in Zr-based glasses in a tensile test; the values of the breaking stress σ_{break} and the flow stress under compression σ_{com} in bulk samples are also shown [47]. (b) Influence of the micropillar diameter on the flow stress under compression in glasses based on Cu (●) and Zr (○) [48].

homogeneous deformation, unlike thicker samples (200 nm or more) subject to brittle fracture with the formation of nonuniform shear bands. This gave the authors of [47] reason to consider the last-mentioned size the region of transition from a strong-yet-brittle to a strong-yet-ductile state.

Phenomenologically, the brittle–ductile behavior under strain can be regarded as the competition between the uniform and nonuniform propagation of shear bands. In the latter case, associated with crack growth, the authors of Ref. [47] used the Griffith method to estimate the influence of diameter on stress necessary for crack propagation. It was shown that the critical diameter of micropillars at which homogeneous deformation occurs is 30–100 nm, in excellent agreement with the above experimental findings (Fig. 7b). The analysis demonstrated that strengthening of the samples with decreasing the diameter (Fig. 7a) is unrelated to the known Weibull size effect (volume-to-strength ratio) and should be attributed to specific effects of shear bands [49].

However, the data in Ref. [47] are confirmed not in all experiments but in just a few designed to elucidate the peculiarities of metallic glass deformation, as is exemplified by Fig. 8b [48] showing that the size of the sample has no effect on the flow stress in micropillars 93–645 nm in diameter under tensile test conditions. In this interval, inhomogeneous deformation was observed, whereas the transition from inhomogeneous to homogeneous strain in bending tests occurred in samples around 200 nm in diameter. A joint review [50] by the principal investigators of studies [47, 48] gives practically no attention to the causes behind these differences, mostly emphasizing numerous conflicting results with the pro/contra ratio of 50:50 (e.g., 'pro' in [51, 52] and 'contra' in [53, 54], etc.). Nevertheless, a decrease in the diameter was shown to be associated with the transition to totally homogeneous deformation in tensile and microbending tests, whereas compression experiments revealed no such deformation [50]. The differences may be due to the dissimilar composition and height/diameter ratio of the study samples, as well as to different experimental conditions, which require a more thorough analysis.

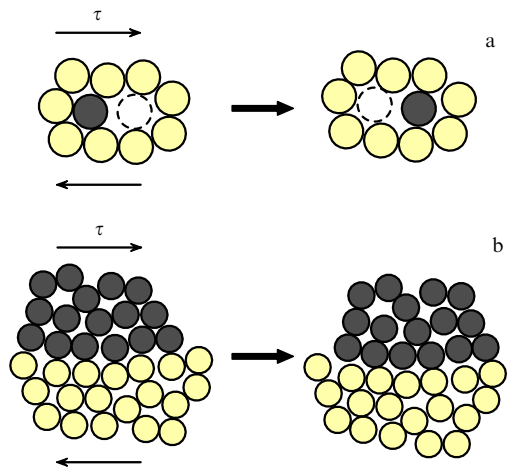

Figure 9. (a) Models of free volume deformation and (b) the shear transformation region [55].

Opinions differ as regards the mechanisms of deformation of metallic nano- and microglasses. It was shown in Ref. [55], focused on the analysis of simulation of localized shear strain in metallic glasses, that integration and correlation of the results of experimental studies, computer simulation, and basic research are needed to fully understand this process. This goal has yet to be reached. Several theoretical concepts were proposed based on the free volume model, one- and two-dimensional models of the shear transformation zone, the assumption of dislocations, etc. [55].

Deformation of metallic glasses is schematically shown in Fig. 9 based on the free volume and shear transformation zone models. Results of computer simulations suggest that an increase in the free volume fraction leads to a decrease in the flow stress. However, the predictive value of the existing theoretical concepts and models is, on the whole, low and needs to be improved. The use of well-attested films of different nanostructures prepared as described in Ref. [39] might be helpful for studying size effects. Equally interesting in this context are multilayer films based on metallic glasses with metal interlayers (e.g., samples of ZrCuTi with nano-

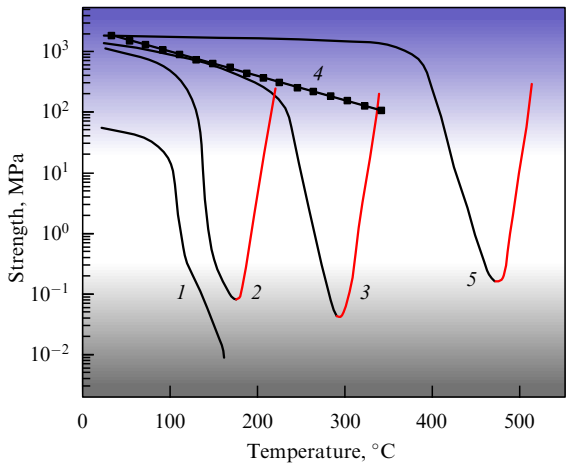

Figure 10. Strength of materials vs temperature: *1* — polymethyl methacrylate, *2* — gold-based BMG, *3* — platinum-based BMG, *4* — nanostructured Ni, *5* — zirconium-based BMG [58].

crystalline Ta layers [56] or $Cu_{50}Zr_{50}/Cu$ nanolaminates [57]). In the latter case, a film was prepared with the ultimate tensile strength $\sigma_B = 2.513$ GPa and a fracture strain of $\sim 4\%$ (the amorphous layer thickness 17–301 nm, the total thickness of the multilayer film 957 ± 89 nm, the best mechanical properties manifested at an amorphous layer thickness of 112 nm). This σ_B value is 33% higher than that deduced from additive considerations based on the starting components and 25% higher than for $Cu_{50}Zr_{50}$ BMG. The authors of [57] argue that the achieved combination of high strength and acceptable ductility is due to a size-dependent deformation of the shear band region in metallic glass interlayers.

3.2 Effects of temperature and ion irradiation

Characteristics of the temperature-dependent evolution of metallic glasses from amorphous to nano- and polycrystalline states were analyzed in Ref. [18] with reference to the possible decay of amorphous phases, the formation of segregations, short-range order changes, alterations of the viscosity, enthalpy, heat capacity, specific volume, and other physicochemical properties. Heating was associated with the passage through characteristic points such as the vitrification temperature (T_g, the temperature of transition from the vitreous state to the viscous flow) and the crystallization temperature (T_c, the melting temperature). The T_c/T_g interval is referred to as the supercooled liquid state interval ΔT; its value is of importance for thermoplastic processing of BMG and the fabrication of intricately shaped articles.

Figure 10 shows temperature dependences of the strength of various (gold-, platinum-, and zirconium-based) BMGs with a characteristic nonmonotonic change in the supercooled interval. For comparison, analogous data are presented for a typical polymer and nanostructured nickel. The polymer (polymethyl methacrylate) is readily processible by extrusion at $T \sim 150\,^\circ$C. Characteristics of gold-based BMG are similar to those of the polymer. Thermoplastic processing of platinum- and zirconium-based BMG with higher T_c and T_g values is possible at higher temperatures, whereas nanostructured Ni is unsuitable for this purpose.

The interesting properties of palladium-based BMG ($Pd_{79}Ag_{3.5}P_6Si_{9.5}Ge_2$) are described in Ref. [59]. It is characterized by the yield strength 1.490 MPa, shear modulus 31 GPa, Poisson coefficient ~ 0.42, $T_g = 613$ K, and the fracture toughness $K_{IC} = 200$ MPa m$^{1/2}$. The strength and toughness fracture of this material are comparable with the respective reference characteristics of steels. Glass of this type is called damage-tolerant glass.

As mentioned in Section 2.1, it was reported in [34–38] that deformation in the shear band region due to the increased temperature and formation of liquid interlayers gave rise to nanostructures such as nanowires, nanofilms, and nanospheres (see Fig. 4). Unfortunately, more detailed information about the influence of temperature on the BMG deformation, to say nothing of nanoglasses, is lacking in the current literature.

The effect of radiation on metallic glasses deserves special discussion. It has recently been considered in many publications with reference to nanomaterials (see reviews [60, 61] and reference 3 therein). Nanostructures undergo beam-induced amorphization as evidenced by the data on ZrO_2, Cu, and Ge nanocrystals implanted into ~ 2 μm thick amorphous layers of silicium dioxide (Table 1) [61]. The structure and composition of initial and irradiated nanoparticles were characterized by several methods, including HRSEM, Rutherford backscattering spectroscopy, small-angle scattering, and X-ray absorption spectroscopy, combined with molecular dynamics simulations.

The most interesting results included in Table 1 pertain to zirconium oxide amorphization (a compound resistant to

Table 1. Effect of irradiation on nanocrystals implanted in the amorphous matrix of SiO_2 (radiation doses are expressed in units of displacement per atom (DPA) and fluence as ions per m^{-2}) [61].

Object	Size of monocrystal, nm	Irradiation conditions				Result
		Ion	Energy E, MeV	Dose, DPA	Fluence, ion m^{-2}	
ZrO_2/SiO_2 [62]	~ 3	Xe	1	0.8		Amorphization
ZrO_2 [63]	Monocrystal	Xe	0.4	680		Crystalline state
Cu/SiO_2 [64, 65]	~ 2.5	Sn	5	0.16		Amorphization
	~ 8	Sn	5		10^{19}	Crystalline state
Au/SiO_2 [62, 66]	3	Xe	1	~ 0.8		Crystalline state
	3 – 5	Sn	2.3		$10^{19} - 10^{20}$	Crystalline state
Ge/SiO_2 [67, 68]	4 – 8	Si	5		$10^{15} - 10^{19}$	Earlier amorphization of nanocrystals
Ge/SiO_2 [69]	3.7 ± 1.0	Au	9		10^{17}	Amorphization

Table 2. Effect of irradiation at room temperature on nanocrystallization of Zr- and C-based metallic glasses [72–75].

Object	Irradiation conditions			Main results
	Ion	E, MeV	Fluence, ion m^{-2}	
$Cu_{50}Zr_{45}Ti_5$ [72]	He	0.14	1.7×10^{13}	Enhanced near-surface hardness at a depth of $\sim$ 600 nm in the nanocrystallization region
$Cu_{50}Zr_{45}Ti_5$ [73]	He	0.14	1.7×10^{13}	Nanocrystallization of $Cu_{10}Zr_7$, $CuZr_2$, and CuZr in irradiated samples. Hardness enhancement similar to that in Ref. [72]
$Zr_{55}Cu_{30}Al_{10}Ni_5$ [74]	Cu	1	10^{12}	Nanocrystallization of $Cu_{10}Zr_7$, $NiZr_2$, and $CuZr_2$ in irradiated samples with bimodal size distribution (5–10 and 50–100 nm)
$Zr_{41.2}Ti_{13.8}Cu_{12.5}Ni_{10}Be_{22.5}$ [75]	Ni	2.5 – 15	10^{12}; doses 0.1 – 100 dpa	Analysis of nanoindentation load curves and the deformation pattern of nanopillars under compression revealed the transition from heterogeneous to homogeneous strain upon increasing the radiation dose

Table 3. Effect of the radiation dose on the yield strength σ_t, the hardness H, and the Young modulus Y on the surface BMG layer ($Zr_{41.2}Ti_{13.8}Cu_{12.5}Ni_{10}Be_{22.5}$) [75].

Radiation dose, dpa	σ_t, GPa	H, GPa	Y, GPa
Initial state	2.18 ± 0.26	7.10 ± 0.17	117.36 ± 1.28
0.1	1.67 ± 0.02	5.87 ± 0.14	108.62 ± 1.47
1	1.82 ± 0.17	5.98 ± 0.19	109.22 ± 2.08
10	1.89 ± 0.1	5.88 ± 0.10	107.85 ± 0.75
100	1.42 ± 0.04	—	—

amorphization in the monocrytalline state even at high radiation doses [63]) and to irradiation of nonamorphizable gold and copper nanocrystals 8 nm in size. As shown in Refs [62, 65, 66], both the size (for Cu) and the nature (for Au) of the object determine the possibility of amorphization of the nanocrystalline state under the effect of irradiation. Detailed observations of irradiated copper nanocrystals revealed the role of Cu_2O formation in amorphization processes [70]. More data on the behavior of irradiated nanoparticles can be found in Ref. [71], where situations differing from those illustrated by Table 1 are considered (e.g., irradiation of Co nanocrystals) and the necessity of further research is emphasized. At the same time, nanoparticles of the metallic glasses being irradiated can show behavior similar to that of metals, semiconductors, and dielectrics included in Table 1.

The influence of ion irradiation on the metallic glass decomposition was discovered long ago (see Ref. [18]), but systematic studies of BMG nanocrystallization are few in number. Results from certain recent publications [72–75] are presented in Table 2. All experiments were conducted at room temperature and its increase under the action of irradiation did not exceed 50 °C [72–74] or 200 °C [75], i.e., it was much lower than T_g. It follows from Table 2 that the results in Refs [72, 73] agree and complement each other. SEM, HRSEM, X-ray structural analysis (XSA), and microdiffraction were used to observe nanocrystallization and to identify the crystalline nanoparticles being formed, whose presence in the structure promotes transition to the plastic state. In this respect, changes in mechanical properties that occur as the radiation dose increases are of special interest (Table 3). A decrease in σ_t, H, and Y along with HRSEM data for micropillars suggest the transition from brittle fracture to plastic deformation. Another important feature of amorphous–nanocrystalline structures is the possibility of enhancing their radiation resistance by increasing the fraction of interfaces as sinks for radiation defects, as shown for many nanomaterials [60, 61].

To summarize, ion irradiation can effectively promote homogeneous deformation of BMGs, increasing their technological ductility. In this context, it would be interesting to compare a variety of methods considered previously for enhancing the BMG ductility, such as annealing, preliminary deformation, the use of single- and multilayer nanocomposites, ion and electron irradiation, doping, and the use of noble metal-based BMGs.

4. Conclusion

The currently available data on the properties of metallic nano- and microglasses are scarce, which does not allow assessing the scope of their applications. But it is clear that they can be used in micro- and nanoelectromechanical systems and various sensing devices for many scientific disciplines, technology, biology, and medicine. The use of BMGs, including traditional magnetic amorphous–crystalline materials, is discussed in general in reviews [21, 76]. Many potential spheres of application are described for thin-film coatings based on metallic glasses, with special reference to such characteristics as antimicrobial properties, small-scale roughness, enhanced durability, and fatigue resistance [77].

Two more aspects are worthy of mention. First, practically all studies on nanoglasses and BMG ductility, except simulation by molecular dynamics methods, are of an experimental and descriptive character without regard for theoretical microscopic concepts in the analysis of one phenomenon or another, e.g., the relation between enhanced ductility and free volume variations. In this context, the proposed composite model of plastic flow of amorphous covalent materials can be of interest as allowing the theoretical consideration of homogeneous nucleation and growth of liquid-like nanoinclusions initiating uniform and nonuniform strain of the entire composite [78]. The microscopic approach can be useful for the elucidation of similarities and differences in the behavior of crystalline nanoparticles and BMGs subjected to ion irradiation (see Tables 1–3). The development of theoretical aspects of nanostructured materials science is an equally topical issue for these objects.

Moreover, it appears that nanostructural principles (see, e.g., [79]) can be more extensively used in developing new materials based on nano- and microglasses and estimating their stability and the role of size effects. On the other hand,

specific behavioral features of thin glass layers are of importance for identifying new properties of nanocomposites like Ti(C,N) – (Ni,Mo), WC – Co, $Si_3N_4 - Al_2O_3 - Y_2O_3$, SiC – TiB_2, and $B_4C - TiB_2$ (see, e.g., [80–83]). Understanding mechanisms of nucleation and growth of nanocrystals at interfaces is indispensable for controlling creep and superplasticity.

The author is grateful to G Gleiter for the enlightening discussion and the gift of reprints. The assistance of V V Klyucharev and S V Klyucharev in the preparation of this review is acknowledged.

The work was supported by the RFBR (grant No. 11-02-92471) and the Program P-8 of the Presidium of the Russian Academy of Sciences.

References

1. Shalnikov A *Nature* **142** 74 (1938)
2. Shal'nikov A I *Zh. Eksp. Teor. Fiz.* **10** 630 (1940)
3. Duwez P, Willens R H, Klement W *J. Appl. Phys.* **31** 1136 (1960)
4. Miroshnichenko I S, Salli I V *Ind. Lab.* **25** 1463 (1959) [*Zavod. Labor.* (11) 1398 (1959)]
5. Salli I V *Fizicheskie Osnovy Formirovaniya Struktury Splavov* (Physical Basis of Formation of Alloy Structure) (Moscow: Metallurgizdat, 1963)
6. Skrishevskii A F *Strukturnyi Analiz Zhidkostei i Amorfnykh Tel* (Moscow: Vysshaya Shkola, 1980)
7. Güntherodt H-J, Beck H *Glassy Metals* Vol. 1 *Ionic Structure, Electronic Transport, and Crystallization* (Berlin: Springer-Verlag, 1981) [Translated into Russian (Moscow: Mir, 1983)]
8. Belashchenko D K *Struktura Zhidkikh i Amorfnykh Metallov* (The Structure of Liquid and Amorphous Metals) (Moscow: Metallurgiya, 1985)
9. Polukhin V A, Vatolin N A *Modelirovanie Amorfnykh Metallov* (Modeling Amorphous Metals) (Moscow: Nauka, 1985)
10. Nemoshkalenko V V et al. *Amorfnye Metallicheskie Splavy* (Amorphous Metallic Alloys) (Exec. Ed. V V Nemoshkalenko) (Kiev: Naukova Dumka, 1987)
11. Luborsky F E (Ed.) *Amorphous Metallic Alloys* (London: Butterworth-Heinemann, 1983) [Translated into Russian (Moscow: Metallurgiya, 1987)]
12. Sudzuki K, Fudzimori H, Hashimoto K *Amorfnye Metally* (Anorphous Metals) (Moscow: Metallurgiya, 1987)
13. Zolotukhin I V, Kalinin Yu V *Sov. Phys. Usp.* **33** 720 (1990) [*Usp. Fiz. Nauk* **160** (9) 75 (1990)]
14. Glezer A M, Molotilov B V *Struktura i Mekhanicheskie Svoistva Amorfnykh Splavov* (The Structure and Mechanical Properties of Amorphous Alloys) (Moscow: Metallurgiya, 1992)
15. Starodubtsev Yu N, Belozerov V Ya *Magnitnye Svoistva Amorfnykh i Nanokristallicheskikh Splavov* (Magnetic Properties of Amorphous and Nanocrystalline Alloys) (Ekaterinburg: Izd. Ural'skogo Univ., 2002)
16. Gantmakher V F *Elektrony v Neuporyadochennykh Sredakh* (Electrons in Disordered Media) (Moscow: Fizmatlit, 2005)
17. Schroers J *Adv. Mater.* **22** 1566 (2010)
18. Abrosimova G E *Phys. Usp.* **54** 1227 (2011) [*Usp. Fiz. Nauk* **181** 1265 (2011)]
19. Glezer A M, Permyakova I E *Nanokristally, Zakalennye iz Rasplava* (Crystals Hardened from the Melt) (Moscow: Fizmatlit, 2012)
20. Gridnev S A et al. *Nelineinye Yavleniya v Nano- i Mikrogeterogennykh Systemakh* (Non-Linear Phenomena in Nano- and Microheterogeneous Systems) (Moscow: Binom. Laboratoriya Znanii, 2012)
21. Andrievskii R A *Bull. Russ. Acad. Sci. Phys.* **76** 37 (2012) [*Izv. Ross. Akad. Nauk Ser. Fiz.* **76** (1) 44 (2012)]
22. Gleiter H, in *Proc. 2nd RISO Symp. on Metallurgy and Materials Science* (Eds S Hansen et al.) (Roskilde: RISO Nat. Lab., 1981)
23. Birringer R et al. *Phys. Lett. B* **102** 365 (1984)
24. Birringer R et al. *Trans. Jpn. Inst. Met. Suppl.* **27** 43 (1986)
25. Gleiter H *Acta Mater.* **56** 5875 (2008)
26. Gleiter H *MRS Bull.* **34** 456 (2009)
27. Gleiter H *Metall. Mater. Trans. A* **40** 1499 (2009)
28. Weissmüller J et al. *Key Eng. Mater.* **77 – 78** 161 (1993)
29. Sopu D et al. *Appl. Phys. Lett.* **94** 191911 (2009)
30. Ritter Y et al. *Acta Mater.* **59** 6588 (2011)
31. Wang X D et al. *Scripta Mater.* **64** 81 (2011)
32. Glezer A M, Gromov V E *Nanokristally, Sozdannye Putem Ekstremal'nykh Vozdeistvii* (Nanocrystals Created Under Extreme Conditions) (Novokuznetsk: Inter-Kuzbass, 2010)
33. Nosova G I et al. *Crystallogr. Rep.* **54** 1058 (2009 [*Kristallografiya* **54** 1111 (2009)]
34. Nakayama K S et al. *Nano Lett.* **8** 516 (2008)
35. Liu Y et al. *Mater. Trans.* **50** 1890 (2009)
36. Xia X-X et al. *J. Mater. Res.* **24** 2966 (2009)
37. Nakayama K S et al. *Adv. Mater.* **22** 872 (2009)
38. Jiang M Q, Duan G H, Dai L H *J. Non-Cryst. Solids* **357** 1621 (2011)
39. Chen N et al. *Acta Mater.* **59** 6433 (2011)
40. Fang J X et al. *Nano Lett.* **12** 458 (2012)
41. Bokeloh J et al. *Phys. Rev. Lett.* **107** 235503 (2011)
42. Tiwari J P, Shahi K *Mater. Sci. Eng. B* **141** 8 (2007)
43. Fang J et al. *Nature Mater.* (2013), in press
44. Gleiter H, in *XI Intern. Conf. on Nanostructured Materials, NANO 2012, Rhodes, Greece, 26 – 31 August, 2012*
45. Andrievski R A, Glezer A M *Phys. Usp.* **52** 315 (2009) [*Usp. Fiz. Nauk* **179** 337 (2009)]
46. Schuh C A, Hufnagel T C, Ramamurty U *Acta Mater.* **55** 4067 (2007)
47. Jang D, Greer J R *Nature Mater.* **9** 215 (2010)
48. Chen C D, Pei Y T, De Hosson J T M *Acta Mater.* **58** 189 (2010)
49. Jang D, Gross C T, Greer J R *Int. J. Plasticity* **27** 858 (2011)
50. Greer J R, De Hosson J T M *Prog. Mater. Sci.* **56** 654 (2011)
51. Lee C J et al. *Appl. Phys. Lett.* **91** 161913 (2007)
52. Bharathula A et al. *Acta Mater.* **58** 5789 (2010)
53. Dubach A et al. *Scripta Mater.* **60** 567 (2009)
54. Wu X L et al. *Acta Mater.* **57** 3562 (2009)
55. Takeuchi Sh, Edagawa K *Prog. Mater. Sci.* **56** 785 (2011)
56. Chou H S et al. *Intermetallics* **19** 1047 (2011)
57. Kim J-Y, Jang D, Greer J R *Adv. Funct. Mater.* **21** 4550 (2011)
58. Kumar G, Tang H X, Schroers J *Nature* **457** 868 (2009)
59. Demetriou M D et al. *Nature Mater.* **10** 123 (2011)
60. Andrievskii R A *Phys. Met. Metallogr.* **110** 229 (2010) [*Fiz. Met. Metalloved.* **110** 243 (2010)]
61. Andrievskii R A *Nanotechnol. Russ.* **6** 357 (2011) [*Ross. Nanotekhnol.* **6** (5 – 6) 34 (2011)]
62. Meldrum A, Boatner L A, Ewing R C *Phys. Rev. Lett.* **88** 025503 (2002)
63. Sickafus K E et al. *J. Nucl. Mater.* **274** 66 (1999)
64. Johannessen B et al. *Appl. Phys. Lett.* **90** 073119 (2007)
65. Johannessen B et al. *Phys. Rev. B* **76** 184203 (2007)
66. Kluth P et al. *Phys. Rev. B* **74** 014202 (2006)
67. Ridgway M C et al. *Phys. Rev. B* **71** 094107 (2005)
68. Djurabekova F et al. *Nucl. Instrum. Meth. Phys. Res. B* **267** 1235 (2009)
69. Sprouster D J et al. *Phys. Rev. B* **81** 155414 (2010)
70. Nita N, Schaeublin R, Victoria M *J. Nucl. Mater.* **329 – 333** 953 (2004)
71. Krasheninnikov A V, Nordlund K *J. Appl. Phys.* **107** 071301 (2010)
72. Carter J et al. *Nucl. Instrum. Meth. Phys. Res. B* **267** 1518 (2009)
73. Xie G et al. *Surf. Coat. Technol.* **206** 829 (2011)
74. Carter J et al. *Nucl. Instrum. Meth. Phys. Res. B* **267** 2827 (2009)
75. Raghavan R et al. *Mater. Sci. Eng. A* **532** 407 (2012)
76. Inoue A, Takeuchi A *Acta Mater.* **59** 2243 (2011)
77. Chu J P et al. *Thin Solid Films* **520** 5097 (2012)
78. Gutkin M Yu, Ovid'ko I A *Phys. Solid State* **52** 58 (2010) [*Fiz. Tverd. Tela* **52** 56 (2010)]
79. Andrievskii R A *Osnovy Nanostrukturnogo Materialovedeniya. Vosmozhnosti i Problemy* (Fundamentals of Nanostructured Materials Science. Potentials and Problems) (Moscow: Binom. Laboratoriya Znanii, 2012)
80. Hampshire S, Pomeroy M J *J. Eur. Ceramic Soc.* **32** 1925 (2012)
81. Belousov V V, Fedorov S V *Russ. Chem. Rev.* **81** 44 (2012) [*Usp. Khim.* **81** 44 (2012)]
82. Gupta N et al. *Mater. Sci. Eng. A* **534** 111 (2012)
83. Liu L et al. *Adv. Mater. Res.* **426** 155 (2012)